2010 IEEE International Conference on Robotics and Automation
Anchorage Convention District
May 3-8, 2010, Anchorage, Alaska, USA

Point-to-Point Motion Control of a Pendulum-like 3-Dof Underactuated Cable-Driven Robot

Simon Lefrançois and Clément Gosselin

Abstract— **This paper presents a novel planar three-degree-of-freedom pendulum-like underactuated robot. The robot consists of an end-effector with an actuated arm suspended on a cable wound on a reel. The robot can achieve full planar point-to-point motion (position and orientation) with zero-velocity landing by swinging itself as children do on playground swings. The equations of motion of the underactuated cable-driven robot are first developed. Then, the actuated joint trajectory design for swing-up as well as an optimization technique used to control the behaviour of the passive joint are proposed. Finally, a prototype of the robot and its real-time controller are presented with experimental results for point-to-point trajectories. The proposed mechanism constitutes a low-cost solution for applications requiring large workspaces by combining the advantages of cable-driven systems and underactuation and, to the best of our knowledge, this is the first work presenting the real-time control of such a mechanism.**

I. INTRODUCTION

Cable-driven robots are well-known solutions for applications requiring large workspaces since cables can be wound on reels, thereby providing large motion ranges. Moreover, replacing rigid links with cables greatly reduces the weight and actuation power. However, cable-driven robots are generally based on parallel architectures with more (or at least as much) actuators than degrees of freedom since cables can only pull and not push. Indeed, implementing such mechanisms requires installing numerous actuators at different locations in space. A support structure as well as some calibration [1] are thereby needed, which drastically increases the implementation costs.

On the other hand, underactuated mechanisms are systems with fewer actuators than degrees of freedom whose control has attracted significant attention. The motion of the free (unactuated) joints is generally related to that of the other joints by complex dynamics, which makes the control problem challenging [2]. Moreover, due to underactuation, only a subset of the kinematically possible global trajectories are achievable. Nevertheless, such mechanisms are very well-suited for point-to-point operations since the latter involve mainly getting from a point to another regardless of the path.

Combining the advantages of underactuation (few actuators, simplicity) with those of cable transmissions (agility, large workspace, low mass) is a promising avenue in order to reduce the cost of large workspace point-to-point operations. Potential applications include dock loading, construction, field robotics, domotics, surveillance systems, automated greenhouses as well as entertainment and human-robot interactions. The latter is possible since underactuated cable-driven robots are lightweight and cannot lead to constrained motions that are a concern in the context of human/robot cooperation [3].

A first two-degree-of-freedom cable-driven pendulum-like robot, referred to as the Winch-Bot, was presented in [4]. The authors used off-line trajectory planning to control the position of the robot. However, the proposed technique requires specific initial conditions that may be incompatible with the architecture or the current configuration of the robot.

The objective of this paper is to present a simple, fully operational 3-dof planar cable-driven underactuated robot and to provide an effective and robust trajectory planning scheme that allows the real-time control of the robot. The planning and control scheme developed in this paper allows the performance of point-to-point trajectories and leads to a natural behaviour of the robot. The proposed mechanism is a 3-dof planar robot whose first R joint is passive, as illustrated in Fig. 1. It consists of an end-effector of length L, mass m_2 and inertia I_2 driven by a motor of mass m_1 and inertia I_1. The centre of mass of the end-effector is located at a distance d_2 from the pivot while the centre of mass of the actuator is located at a distance d_1 from the same pivot. The actuator is maintained in line with the cable using a

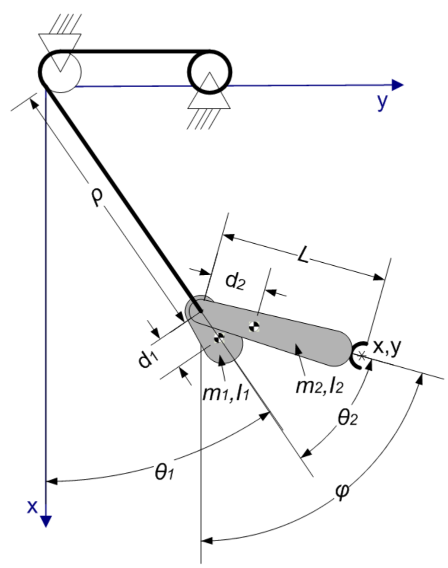

Fig. 1. The three-degree-of-freedom underactuated cable-driven robot.

This work was supported by The Natural Sciences and Engineering Research Council of Canada (NSERC) and by the Canada Research Chair Program.

The authors are with the Department of Mechanical Engineering, Université Laval, 1065 Ave. de la médecine, Québec, Québec. Canada, G1V 0A6, simon.lefrancois.1@ulaval.ca, gosselin@gmc.ulaval.ca

978-1-4244-5040-4/10/$26.00 ©2010 IEEE

rigid section at the end of the latter. The angle of the cable with respect to a vertical axis is noted θ_1 while the angle between the cable and the end-effector is noted θ_2. Angle θ_2 is associated with the suspended motor while angle θ_1 is an unactuated coordinate. The end-effector motor is suspended to a cable of length ρ passing through a pulley and wound on a reel actuated by a second fixed motor. Therefore, the length of the cable can be controlled using the latter actuator. Globally, the mechanism can be thought of as a planar serial RPR robot whose first R joint is not actuated.

Based on the physical properties of the pendulum system formed by the robot, a trajectory planning scheme is developed and a real-time optimization algorithm is used to control the behaviour of the unactuated joint. The robot can achieve planar point-to-point motion (position and orientation) with zero-velocity landing by swinging itself as children do on playground swings. It uses both techniques pointed out by Case [5],[6] for effective swinging, namely, i) leg-stretching as in seated swinging, using end-effector swing and ii) centre of mass motion as in standing swinging, using cable extension. Moreover, the proposed control technique does not require specific initial conditions.

The rest of this paper is structured as follows: first, the equations of motion of the underactuated cable-driven robot are developed. Then, the actuated joint trajectory design for swing-up as well as an optimization technique used to control the behaviour of the unactuated joint are proposed. A prototype of the robot and its real-time controller are also presented with experimental results for point-to-point trajectories. Finally, the future development of $x-y$ path-tracking trajectories is briefly addressed.

II. Equations of Motion

In this section, the kinematic and dynamic equations governing the motion of the underactuated 3-dof cable-driven robot are obtained.

A. Kinematics

Referring to Fig. 1, the direct kinematics of the robot can be written as:

$$\begin{aligned} x &= \rho\cos\theta_1 + L\cos(\theta_1+\theta_2) \\ y &= \rho\sin\theta_1 + L\sin(\theta_1+\theta_2) \\ \phi &= \theta_1+\theta_2. \end{aligned} \tag{1}$$

From these equations, the solution of the inverse kinematic problem is readily obtained as:

$$\begin{aligned} \theta_1 &= \operatorname{atan2}\left(\frac{y-L\sin\phi}{\rho}, \frac{x-L\sin\phi}{\rho}\right) \\ \rho &= \sqrt{(x-L\cos\phi)^2+(y-L\sin\phi)^2} \\ \theta_2 &= \phi-\theta_1. \end{aligned} \tag{2}$$

B. Dynamics

In order to simplify the dynamic model, it is first assumed that the cable is a massless rigid body. This implies that tension T in the cable is always sufficient to avoid sagging. Moreover, friction in guides and pulleys as well as aerodynamic effects are neglected compared to the other forces in the system. Then, using Lagrangian dynamics, the equations of motion can be obtained and written as:

$$\begin{aligned} &\left(I_1+I_2+m_1(\rho+d_1)^2+m_2(\rho+d_2\cos\theta_2)^2\right)\ddot{\theta}_1 \\ &\quad -m_2d_2\sin\theta_2\ddot{\rho}+\left(I_2+m_2(d_2^2+\rho d_2\cos\theta_2)\right)\ddot{\theta}_2 \\ &\quad +2\left(m_1\left(\rho+d_1\right)+m_2\left(\rho+d_2\cos\theta_2\right)\right)\dot{\rho}\dot{\theta}_1 \\ &\quad -m_2\rho\dot{\theta}_2\sin\theta_2\left(2\dot{\theta}_1+\dot{\theta}_2\right)+m_1g\left(\rho+d_1\right)\sin\theta_1 \\ &\quad +m_2g\left(\rho\sin\theta_1+d_2\sin\left(\theta_1+\theta_2\right)\right) = 0 \end{aligned} \tag{3}$$

$$\begin{aligned} &m_2d_2\sin\theta_2\left(\ddot{\theta}_1+\ddot{\theta}_2\right)-\left(m_1+m_2\right)\ddot{\rho} \\ &\quad +\left(m_1\left(\rho+d_1\right)+m_2\rho\right)\dot{\theta}_1^2 \\ &\quad +m_2d_2\cos\theta_2\left(\dot{\theta}_1+\dot{\theta}_2\right)^2+\left(m_1+m_2\right)g\cos\theta_1 = T \end{aligned} \tag{4}$$

$$\begin{aligned} &\left(I_2+m_2\left(d_2^2+\rho d_2\cos\theta_2\right)\right)\ddot{\theta}_1-m_2d_2\sin\theta_2\ddot{\rho} \\ &\quad +\left(m_2d^2+I_2\right)\ddot{\theta}_2+2m_2d_2\dot{\rho}\dot{\theta}_1\cos\theta_2 \\ &\quad +m_2d_2\rho\dot{\theta}_1^2\sin\theta_2+m_2d_2g\sin(\theta_1+\theta_2) = \tau \end{aligned} \tag{5}$$

where m_i, I_i and d_i are respectively the mass, inertia and location of the centre of mass of body i, T is the tension in the cable, τ is the torque applied by the motor mounted at the end of the cable and g is the gravitational acceleration.

Equation (3) is the most relevant motion equation of this system since it does not include any control input as there is no actuator at the first joint. Equations (4) and (5) will be used to compute the actuator force and torque and to verify that the tension is positive in the cable and that the actuator torque is within its limits.

III. Trajectory Planning

From the dynamic model presented in the above section, and for given initial conditions, cable angle $\theta_1(t)$ can be predicted for known trajectories of the actuated joints $\rho(t), \theta_2(t)$ by integrating (3). However, for the prediction to be correct, the prescribed trajectories must also satisfy the following conditions:

1) Positive tension is maintained
2) Actuator torque and joint limits are satisfied
3) Joint trajectories and their derivatives are smooth, to prevent shocks
4) Prediction time is small enough so that the computational burden and the model errors are bounded.

From the latter point, it is clear that planning entire trajectories from zero initial conditions to large cable angles would be very difficult. On the other hand, since the motion of the robot is governed by pendulum-like dynamics, planning trajectories over half-periods of oscillation is appropriate since the prediction horizon is relatively small and the dynamics are similar in-between zero-velocity states $\left(\dot{\theta}_1=0\right)$.

A. Trajectory of the Unactuated Joint

Defining a goal $[x_g, y_g, \phi_g]$ to be reached with a zero final velocity, joint coordinates $[\theta_{1g}, \rho_g, \theta_{2g}]$ are obtained from (2). Since the actuated joint goals are easily reachable, the objective is to find actuated joint trajectories that allow the robot to reach the desired cable angle or, at least, within half a period, a cable angle which is closer to the prescribed goal. These trajectories must also satisfy initial conditions to maintain continuity and final conditions that satisfy the objectives. Since the system is governed by complex dynamics, it is clear that optimal trajectories are not obtainable within acceptable computation time.

Thus, a technique similar to the one presented by Tortopidis and Papadopoulos [7] for underactuated space manipulators will be used here. Indeed, trajectories defined using $p+q$ parameters are used together with p boundary conditions on each actuated joint thereby leaving q free parameters. These free parameters can then be tuned through optimization in order to produce the desired underactuated joint behaviour. Here, there are $p = 6$ boundary conditions (initial/final positions, velocities and accelerations) and, for simplicity reasons, $q = 1$ free parameter is left for each actuated joint.

Since a zero velocity is desired at the target configuration (for smooth landing), extrema of θ_1 are considered as starting/ending point of trajectories. This leads to a cosine-like function for $\theta_1(t)$ on a half-period. Moreover, since a large workspace is desired, large values of θ_1 must be reachable and the robot must be able to efficiently excite itself to achieve such motions. Special attention must then be given to trajectory planning and this will be addressed for each actuated joint independently.

B. Cable Extension

Considering a lumped end-effector (no actuator mounted at the end of the cable), the system becomes similar to a variable-length (Lorentz) pendulum whose swing-up motion was studied in [8],[9]. It was suggested by Burns [10] and proven optimal for instantaneous variation of length by Piccoli and Kulkarni [11] that lengthening the cable when the angular velocity of the cable is minimum and shortening it when the angular velocity is maximum amplifies the system's energy.

Hence, given the mathematical form of θ_1 prescribed above, a sine-like function is choosen for the cable extension. As shown in Fig. (2) —which was obtained through numerical simulation—, exciting the system at twice its natural frequency with a $\pm\pi/2$ phase from cable angle position is best-suited to increase (or decrease) the cable angle, which is consistent with Burns' results [10]. Since the cable angle describes a cosine-like function between two zero-velocity states ($\dot{\theta}_1 = 0$), the following function is chosen for the cable extension:

$$\begin{aligned} \rho(t) &= A_1 \sin(2\omega t) + B_1 \sin(3\omega t) + C_1 \sin(4\omega t) \\ &\quad + \rho_i + \frac{(\rho_f - \rho_i)\,\omega t}{\pi} \end{aligned} \tag{6}$$

for $0 \le t \le \pi/\omega$.

In (6), indices i and f refer to initial/final conditions, t is the time, ω is the system's natural frequency and A_1 is a free parameter which is optimized for each half-period in order to control the behaviour of angle θ_1. Coefficients B_1 and C_1 are obtained by prescribing the time derivative of (6) at times $t = 0$ and $t = \pi/\omega$ to be equal to the initial/final velocities $\dot{\rho} = \dot{\rho}_i$ and $\dot{\rho} = \dot{\rho}_f$. This leads to:

$$B_1 = \frac{\dot{\rho}_i - \dot{\rho}_f}{6\omega} \tag{7}$$

$$C_1 = -\frac{A_1}{2} + \frac{\rho_i - \rho_f}{4\pi} + \frac{\dot{\rho}_i + \dot{\rho}_f}{8\omega}. \tag{8}$$

For stability reasons, the boundary condition on accelerations are chosen to be zero by definition of (6). Initial conditions are measured from encoders while final conditions are defined as follows:

$$\rho_f = \begin{cases} \rho_g & \text{if} \quad |\rho_g - \rho_i| < \Delta\rho_{max} \\ \rho_i + \Delta\rho_{max} & \text{else if} \quad \rho_g > \rho_i \\ \rho_i - \Delta\rho_{max} & \text{else} \end{cases} \tag{9}$$

$$\dot{\rho}_f = \begin{cases} 0 & \text{if} \quad |\rho_g - \rho_i| < \Delta\rho_{max} \\ & \quad \text{and } \theta_{1p} = \theta_{1g} \\ 2\omega A_1 & \text{else} \end{cases} \tag{10}$$

where ρ_g is the target cable length and $\Delta\rho_{max}$ is the maximal cable length variation allowed by the maximum velocity of the actuator. Hence, a target cable length is set at first and maintained until the target cable angle θ_{1g} is reached. The final velocity is chosen to match the basic sine conditions in order to limit accelerations and is set to zero for smooth landing when the target point is reached.

C. End-Effector Swing

On the other hand, considering a fixed-length cable, the problem becomes similar to a double pendulum with a long first link. The swing-up problem of a double-pendulum

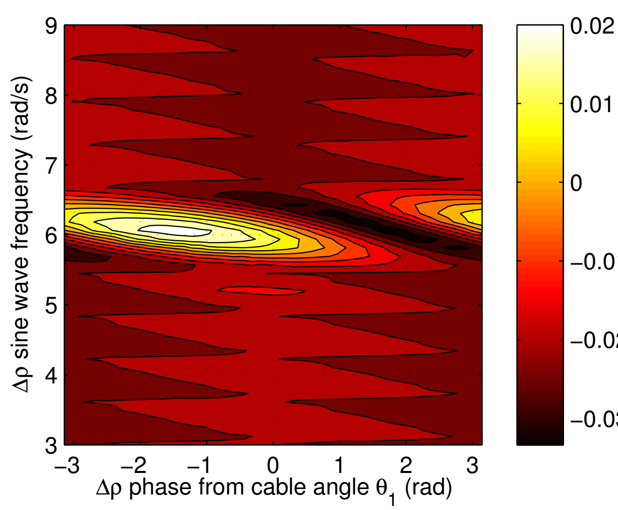

Fig. 2. Average amplitude gain for θ_1 by half-period for cable extension $\omega_n = 3.05(rad/s), \bar{\rho} = 1(m), \Delta\rho = 0.05(m), \theta_2 = 0(rad)$.

with a passive first joint was widely studied in the context of the Acrobot [12],[13],[14] and Brachiation Robots [15]. Spong [12] suggests that, in order to increase the system energy, the motion of the lower link must be "in-phase" with the upper link. Thus, a sine-like function is chosen for the end-effector swing since the upper link motion is of this form. As shown in Fig. (3) —which was obtained through numerical simulation—, exciting the system at its natural frequency is best-suited to increase (or decrease) the cable angle, as pointed out by Spong. A phase of $-3\pi/4$ or $\pi/4$ from the cable angle is also preferable. However, in order to synchronize the goal-reaching with the cable extension and to impose zero boundary acceleration from the outset, a sine function with a phase of $\pm\pi/2$ is chosen since it produces almost the same amplitude of excitation. Therefore, the following function was chosen for the end-effector swing:

$$\begin{aligned}\theta_2(t) &= A_2 \sin(\omega t) + B_2 \sin(2\omega t) + C_2 \sin(3\omega t) \\ &\quad + \theta_{2i} + \frac{(\theta_{2f} - \theta_{2i})\,\omega t}{\pi} \end{aligned} \tag{11}$$

for $0 \le t \le \pi/\omega$.

Similarly to A_1, A_2 is a free parameter used to adjust the behaviour of angle θ_1. Also, coefficients B_2 and C_2 are obtained by prescribing the time derivative of (11) at times $t = 0$ and $t = \pi/\omega$ for initial/final velocities $\dot{\theta}_2 = \dot{\theta}_{2i}$ and $\dot{\theta}_2 = \dot{\theta}_{2f}$. This leads to:

$$B_2 = \frac{\theta_{2i} - \theta_{2f}}{2\pi} + \frac{\dot{\theta}_{2i} + \dot{\theta}_{2f}}{4\omega} \tag{12}$$

$$C_2 = -\frac{A_2}{3} + \frac{\dot{\theta}_{2i} - \dot{\theta}_{2f}}{6\omega}. \tag{13}$$

For stability reasons, the boundary conditions on accelerations are chosen to be zero by definition of (11). Initial conditions are measured from encoders while final conditions are defined as follows:

$$\begin{bmatrix} \theta_{2f} \\ \dot{\theta}_{2f} \end{bmatrix} = \begin{cases} [\theta_{2g}, 0]^T & \text{if } |\rho_g - \rho_i| < \Delta\rho_{max} \text{ and } \theta_{1p} = \theta_{1g} \\ [0, -\omega A_2]^T & \text{else} \end{cases} \tag{14}$$

Similarly to the cable length, the final velocity is chosen here to match the basic sine conditions in order to limit accelerations and is set to zero for smooth landing when the target point is reach. Since θ_{2g} is always reachable within a half-period, θ_{2f} is kept to zero for symmetry reasons until the goal is reached.

IV. Optimization of the Free Joint Trajectory

As pointed out before, one free parameter A_j is used for each actuated joint in order to adjust the behaviour of angle θ_1. However, since the robot dynamics are complex, there is no analytical equation defining $\theta_1(t)$ from the actuated joint trajectories. Indeed, it must be predicted by integrating (3) in real-time.

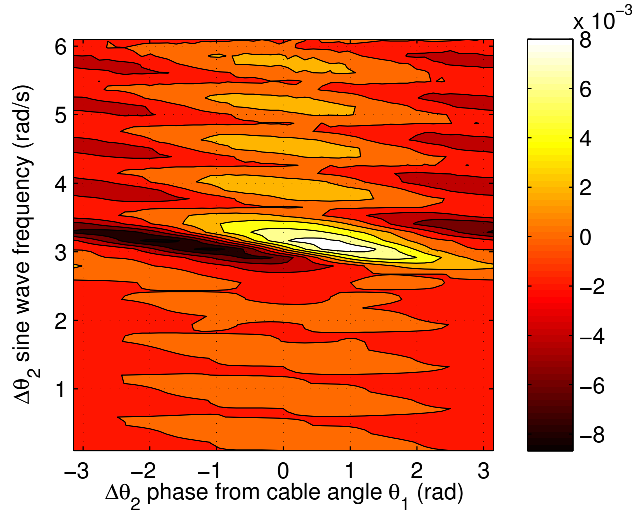

Fig. 3. Average amplitude gain for θ_1 by half-period for end-effector swing $\omega_n = 3.05(rad/s), \rho = 1(m), \bar{\theta}_2 = 0(rad), \Delta\theta_2 = \pi/2(rad)$.

A. Optimization Function

The main objective is to minimize the difference between the cable angle prediction θ_{1p} and its desired value θ_{1g} using the free parameters (A_1, A_2) whose values can be tuned without modifying the actuated joints' final positions.

However, A_1 and A_2 affect the tension, the torque, the joint maximal positions as well as the velocities, which must be considered in the optimization. Indeed, fulfilling the associated constraints must also be included in the optimization function. This is accomplished here using penalty functions, which are chosen to be combinations of ramps and step-functions as follows:

$$P_j = \begin{cases} 0 & \text{if } \eta_j \le \eta_{j,max} \\ K_1 + K_2(\eta_j - \eta_{j,max}) & \text{else} \end{cases} \tag{15}$$

where P_j is the penalty function associated to constraint η_j, $\eta_{j,max}$ is the maximal allowed value for this constraint and K_1, K_2 are positive constants tuned experimentally. Constraints include joint positions, velocities and accelerations as well as cable tension and end-effector torque. Thus, the optimization function is defined as:

$$\min_{A_1, A_2} \Delta, \text{ with } \Delta = (|\theta_{1g}| - |\theta_{1p}|)^2 + \sum_{j=1}^{c} P_j \tag{16}$$

where c is the total number of constraints.

In this equation, the absolute value of the cable angle is used since, from the pendulum-like dynamics, values of θ_{1p} will vary from positive to negative within each half-period.

B. Optimization Algorithm

For each step of the optimization process, given (A_1, A_2), the optimization function can be computed using results obtained by integrating (3). For solving in real-time, the Nelder-Mead algorithm [16] is used since it requires no derivative which, for our problem, can only be computed through finite differences. Moreover, this algorithm is fast and convergence is guaranteed for strictly convex functions. The three starting points needed for the algorithm are chosen to be:

$$\begin{aligned}(A_1, A_2)_1 &= \left(\frac{-\dot{\rho}_{max}}{4\omega}, \frac{\theta_{2max}}{2}\right)\\ (A_1, A_2)_2 &= \left(\frac{-\dot{\rho}_{max}}{4\omega}, \frac{-\theta_{2max}}{2}\right)\\ (A_1, A_2)_3 &= \left(\frac{\dot{\rho}_{max}}{4\omega}, \frac{\theta_{2max}}{2}\right). \end{aligned} \quad (17)$$

When included in (6) and (11) for standard initial/final conditions, these values correspond to reaching approximately half of maximum cable velocity and half of maximal end-effector angle which are associated with the most restrictive penalty functions. Thus, the starting solutions are located in the middle of the penalty-free zone which accelerates the algorithm's convergence.

C. Frequency Determination

As described in section III, the trajectories are defined as functions of the system's natural frequency. However, the natural frequency is also a function of the cable length ρ. Hence, the natural frequency must be determined while performing optimization for the system to be well-synchronized, i.e., for the goals for each joint to be reached simultaneously.

Since no analytical function is available to define the system's frequency, it must be computed while integrating equations of motion. Since the half-period on which optimization is performed is defined from zero-velocity states, the frequency is obtained by finding the time of the next zero velocity point $\left(\dot{\theta}_1 = 0\right)$. Then, the actuated joint trajectories are defined using the latter frequency and the optimization algorithm is started. Moreover, the frequency is re-computed throughout the algorithm since it is also a slow-varying function of (A_1, A_2).

V. Implementation

A small prototype of the underactuated robot was built as shown in Fig. 4 with the specifications presented in Table I. The latter were obtained either by direct measurements or CAD analysis and the robot was designed using a parallelogram shape to ensure planar motion. DC motors with encoders are used to actuate and measure both the end-effector and the cables which are both wound on a single reel to ensure that they have the same length. The cable angle θ_1 is measured using encoders mounted on the robot's supporting pulleys.

A controller was implemented on a real-time QNX computer with a servo-rate of 500 Hz. Closed-loop PID were used to control the actuated joint positions and a 12-step fixed-step fourth order Runge-Kutta formula [17] was used to integrate the equations of motion. $M = 4$ iterations of the Nelder-Mead algorithm were computed for each step and a total of $N = 6$ steps (0.012s) were used to define the free-parameters (A_1, A_2). Nevertheless, even through

Fig. 4. Prototype of the 3-dof underactuated cable-driven robot.

TABLE I
Specifications of the prototype

Description		$i = 1$	$i = 2$
Mass	m_i (kg)	1.291	0.404
Inertia	I_i (kgm^2)	4.0×10^{-3}	4.8×10^{-3}
Location of CoM	d_i (m)	0.046	0.033
End-Effector Length	L (m)	0.300	

optimization, the closed-loop PID is operated at 500 Hz. The structure of the controller is shown in Fig. 5.

At each time step k, if the number of steps performed n is less than maximum number N, an M-iteration optimization algorithm including the definition of parameters (A_1, A_2), the integration of the equations of motion, the frequency computation and the computation of the optimization function, is started using the previous values of (A_1, A_2) as a

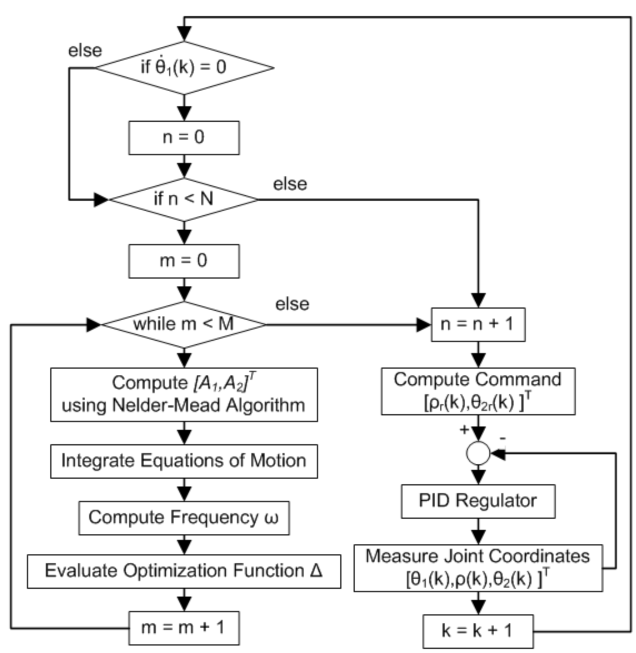

Fig. 5. Controller structure for an N-step, M-iteration-by-step controller.

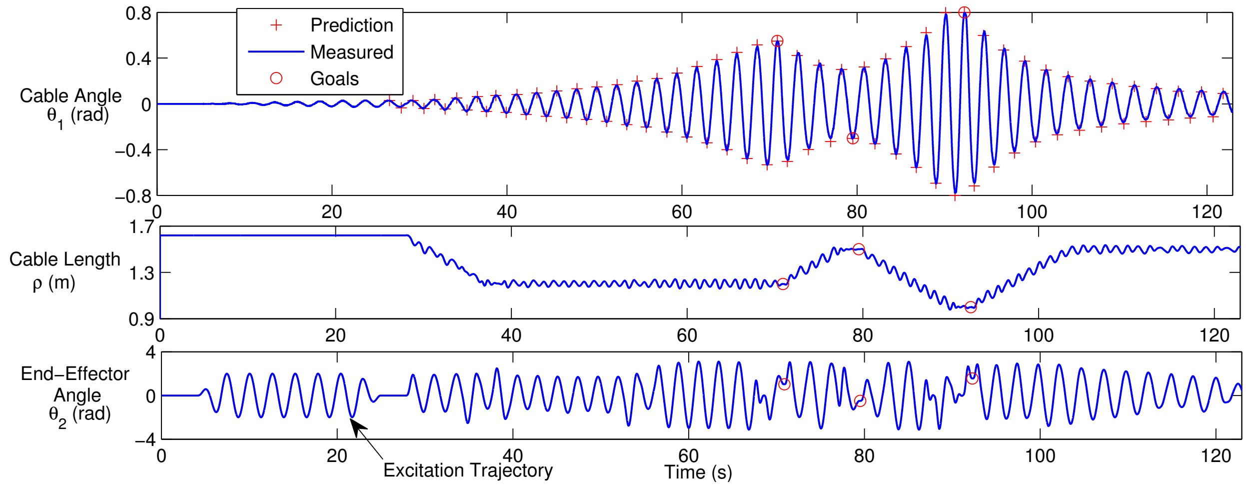

Fig. 6. Joints trajectories for point-to-point motion

starting point. Then, the desired trajectories are sent to a PID controller driving the actuators. The joint coordinates are measured and the next time step is processed. The number of steps performed is reset to zero and starting points from (17) are used when zero-velocity is reached for the cable angle.

In practice, it was difficult to make predictions for small cable angles since the dynamics are slightly different [18]. Indeed, when θ_1 is small, the system is more subject to cable flexion and vibrations. Therefore, pre-designed excitation trajectories with fixed amplitude and frequency were used for end-effector swing in order to initiate the motion.

A. Experimental results

A series of end-effector Cartesian coordinates $[x_i, y_i, \phi_i]^T$, for $i = 1..r$ simulating point-to-point trajectories are used to evaluate performances. Points were chosen to include increasing and decreasing amplitudes of θ_1 as well as shortening and lengthening of the cable.

Using the controller structure and the trajectory planning described above, actuated joint trajectories and cable angle predictions were computed in real-time for these objectives. Fig. 6 presents joint trajectories for point-to-point motion, Fig. 7 presents cable angle prediction vs. measurements for the goal region and Fig. 8 presents cable angle prediction errors. The robot motion from which these graphs were obtained can be seen in the accompanying video.

Cable angle predictions for the underactuated robot were generally sufficient for great controllability. Goal-reaching precision was excellent since joint motions were well-synchronized with the frequency estimation for pick-and-place actions. Predictions were sligthly less accurate when decreasing the system's energy since the tension in the cable was then reduced. This causes off-axis rotations which cannot be predicted by our model. Nevertheless, the experimental results were sufficient to confirm the accuracy of the method presented above.

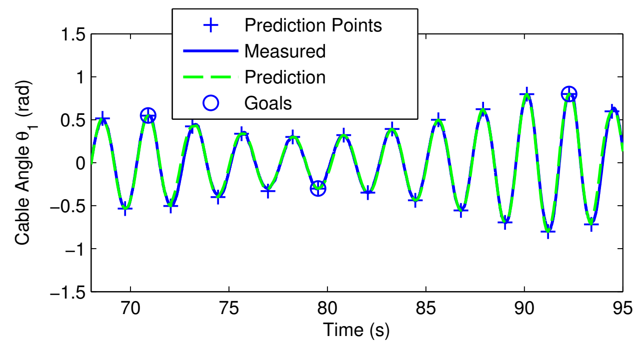

Fig. 7. Cable angle prediction in goal region for point-to-point motion

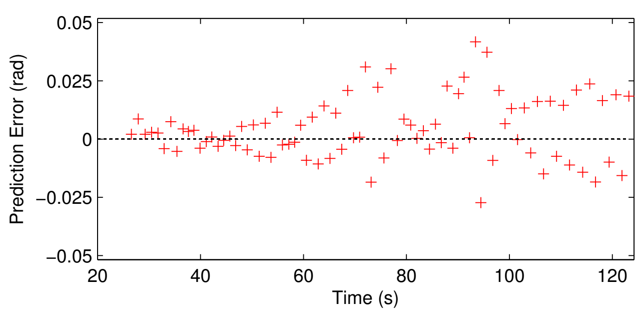

Fig. 8. Cable angle prediction error for point-to-point motion

VI. Future Work

The next step in our project is to perform $x-y$ path-tracking trajectories. Even if the system is limited by underactuation, it is still overdetermined for 2-dof positioning tasks which gives great flexibility for complex operations. It is now planned to develop a method defining path-following trajectories for actuated and unactuated joints by choosing the best possible initial conditions and optimizing path control. Initial conditions can be obtained using the point-to-point controller presented above and path-tracking can be accomplished similarly by combining path points in a global objective.

VII. Conclusion

A three-degree-of-freedom planar robot combining the advantages of cable-driven actuation and underactuation was presented. The actuated joint trajectory design for swing-up as well as an optimization technique used to control the behaviour of the free joint were presented. Actuator and joint limitations as well as positive tension were also included in the problem. Finally, a small prototype of the robot and its real-time controller were presented. It was shown through experimentation that the strategy developed was successful at reaching objectives and that precision was sufficient for point-to-point trajectories. Further developments on $x - y$ path-tracking trajectories was also discussed.

References

[1] P. Bosscher, R. II, and M. Tummino, "A concept for rapidlydeployable cable robot search and rescue systems," *in 2005 Proceedings of the ASME IDETC/CIE, Long Beach CA, USA*, pp. 1–10, 2005.

[2] I. Fantoni and R. Lozano, *Non-linear control for underactuated mechanical systems*. Springer Verlag, 2001.

[3] S. Haddadin, A. Albu-Schaffer, M. Frommberger, and G. Hirzinger, "The role of the robot mass and velocity in physical human-robot interaction-Part II: Constrained blunt impacts," *in 2008 Proceedings of the IEEE International Conference on Robotics and Automation, Pasadena CA, USA*, pp. 1339–1345, 2008.

[4] D. Cunningham and H. Asada, "The Winch-Bot: A Cable-Suspended, Under-Actuated Robot Utilizing Parametric Self-Excitation," *in 2009 Proceedings of the IEEE International Conference on Robotics and Automation, Kobe, Japan*, pp. 1844–1850, 2009.

[5] W. Case, "The pumping of a swing from the standing position," *American Journal of Physics*, vol. 64, p. 215, 1996.

[6] W. Case and M. Swanson, "The pumping of a swing from the seated position," *American Journal of Physics*, vol. 58, p. 463, 1990.

[7] I. Tortopidis and E. Papadopoulos, "On point-to-point motion planning for underactuated space manipulator systems," *Robotics and Autonomous Systems*, vol. 55, no. 2, pp. 122–131, 2007.

[8] S. Curry, "How children swing," *American Journal of Physics*, vol. 44, p. 924, 1976.

[9] M. Pinsky and A. Zevin, "Oscillations of a pendulum with a periodically varying length and a model of swing," *International Journal of Non Linear Mechanics*, vol. 34, no. 1, pp. 105–110, 1999.

[10] J. Burns, "More on pumping a swing," *American Journal of Physics*, vol. 38, p. 920, 1970.

[11] B. Piccoli and J. Kulkarni, "Pumping a swing by standing and squatting: do children pump time optimally?," *IEEE Control Systems Magazine*, vol. 25, no. 4, pp. 48–56, 2005.

[12] M. Spong, "The swing up control problem for the acrobot," *IEEE Control Systems Magazine*, vol. 15, no. 1, pp. 49–55, 1995.

[13] S. Brown and K. Passino, "Intelligent control for an acrobot," *Journal of Intelligent and Robotic Systems*, vol. 18, no. 3, pp. 209–248, 1997.

[14] G. Boone, "Minimum-time control of the acrobot," *in 1997 Proceedings of the IEEE International Conference on Robotics and Automation, Albuquerque NM, USA*, pp. 111–111, 1997.

[15] J. Nakanishi, T. Fukuda, and D. Koditschek, "A brachiating robot controller," *IEEE Transactions on Robotics and Automation*, vol. 16, no. 2, pp. 109–123, 2000.

[16] J. Lagarias, J. Reeds, M. Wright, and P. Wright, "Convergence properties of the Nelder-Mead simplex method in low dimensions," *SIAM Journal on Optimization*, vol. 9, no. 1, pp. 112–147, 1999.

[17] F. Scheid, *Schaum's outline of theory and problems of numerical analysis*. Schaum's Outline Series, 1989.

[18] B. Gore, "Starting a swing from rest," *American Journal of Physics*, vol. 39, p. 347, 1971.